

An ultrafast and low-power slow light tuning mechanism for compact aperture-coupled disk resonators

Bo-Yun Wang(王波云), Yue-Hong Zhu(朱月红), Jing Zhang(张静), Qing-Dong Zeng(曾庆栋), Jun Du(杜君), Tao Wang(王涛), Hua-Qing Yu(余华清)

Citation: Chin. Phys. B . 2020, 29(8): 084211 . **doi:** 10.1088/1674-1056/ab9df1
Journal homepage: http://cpb.iphy.ac.cn; http://iopscience.iop.org/cpb

What follows is a list of articles you may be interested in

Multi-window transparency and fast-slow light switching in a quadratically coupled optomechanical system assisted with three-level atoms

Wan-Ying Wei(魏晚迎), Ya-Fei Yu(於亚飞), Zhi-Ming Zhang(张智明)
Chin. Phys. B . 2018, 27(3): 034204 . **doi:** 10.1088/1674-1056/27/3/034204

Broadrange tunable slow and fast light in quantum dot photonic crystal structure

Alireza Lotfian, Reza Yadipour, Hamed Baghban
Chin. Phys. B . 2017, 26(12): 124207 . **doi:** 10.1088/1674-1056/26/12/124207

Ghost imaging with broad distance

Duan De-Yang, Zhang Lu, Du Shao-Jiang, Xia Yun-Jie
Chin. Phys. B . 2015, 24(10): 104203 . **doi:** 10.1088/1674-1056/24/10/104203

Vacuum induced transparency and slow light phenomena in a two-level atomic ensemble controlled by a cavity

Guo Yu-Jie, Nie Wen-Jie
Chin. Phys. B . 2015, 24(9): 094205 . **doi:** 10.1088/1674-1056/24/9/094205

Image information transfer via electromagnetically induced transparency-based slow light

Wang Xiao-Xiao, Sun Jia-Xiang, Sun Yuan-Hang, Li Ai-Jun, Chen Yi, Zhang Xiao-Jun, Kang Zhi-Hui, Wang Lei, Wang Hai-Hua, Gao Jin-Yue
Chin. Phys. B . 2015, 24(7): 074204 . **doi:** 10.1088/1674-1056/24/7/074204

An ultrafast and low-power slow light tuning mechanism for compact aperture-coupled disk resonators*

Bo-Yun Wang(王波云)[1,†], Yue-Hong Zhu(朱月红)[1], Jing Zhang(张静)[1], Qing-Dong Zeng(曾庆栋)[1], Jun Du(杜君)[1], Tao Wang(王涛)[2], and Hua-Qing Yu(余华清)[1,‡]

[1] School of Physics and Electronic-information Engineering, Hubei Engineering University, Xiaogan 432000, China
[2] Wuhan National Laboratory for Optoelectronics, Huazhong University of Science and Technology, Wuhan 430074, China

(Received 6 April 2020; revised manuscript received 7 May 2020; accepted manuscript online 18 June 2020)

An ultrafast and low-power slow light tuning mechanism based on plasmon-induced transparency (PIT) for two disk cavities aperture-coupled to a metal-dielectric-metal plasmonic waveguide system is investigated numerically and analytically. The optical Kerr effect is enhanced by the local electromagnetic field of surface plasmon polaritons, slow light, and graphene–Ag composite material structures with a large effective Kerr nonlinear coefficient. Through the dynamic adjustment of the frequency of the disk nanocavity, the group velocity is controlled between $c/53.2$ and $c/15.1$ with the pump light intensity increased from 0.41 MW/cm^2 to 2.05 MW/cm^2. Alternatively, through the dynamic adjustment of the propagation phase of the plasmonic waveguide, the group velocity is controlled between $c/2.8$ and $c/14.8$ with the pump light intensity increased from 5.88 MW/cm^2 to 11.76 MW/cm^2. The phase shift multiplication of the PIT effect is observed. Calculation results indicate that the entire structure is ultracompact and has a footprint of less than 0.8 μm^2. An ultrafast responsive time in the order of 1 ps is reached due to the ultrafast carrier relaxation dynamics of graphene. All findings are comprehensively analyzed through finite-difference time-domain simulations and with a coupling-mode equation system. The results can serve as a reference for the design and fabrication of nanoscale integration photonic devices with low power consumption and ultrafast nonlinear responses.

Keywords: slow light, plasmon-induced transparency (PIT), graphene, plasmonic waveguide

PACS: 42.50.Gy, 42.15.Eq, 42.65.Wi, 81.05.ue **DOI:** 10.1088/1674-1056/ab9df1

1. Introduction

Slow light is a crucial element in the study of quantum information processing, optical communication, and all-optical storage. The effective realization of slow light depends on the development of electromagnetically induced transparency (EIT). Quantum destructive interference between the excitation pathways to the atomic upper level indicates that the peculiar and counter-intuitive phenomenon called EIT has appeared in the atomic system.[1] EIT performance in transparent windows with strong dispersion and enhanced transmitted characteristics[2] indicates that EIT can be widely used in enhanced optical nonlinearity, optical data storage, and sensors. The potential application of the EIT effect is obstructed by its requirements of extreme cold environments and stable gas lasers. Nevertheless, researchers have demonstrated that plasmon-induced transparency (PIT) can be obtained in photonic nanostructures.[3] The PIT effect is similar to the classical EIT and has attracted extensive attention due to its potential for use in information-processing chips and integrated photonic devices.[4] The PIT effect causes a strong destructive interference between narrowband dark and wideband bright patterns.[5] As a particular case of Fano resonance, the PIT effect with steep dispersion decreases the group velocity.[6] The enhancement capability is large in accordance with the local electromagnetic (EM) field, and the typical diffraction limit caused by surface plasmon polaritons (SPPs) is solved; thus, a device based on the PIT effect can be used with a small footprint.[7] The PIT effects on plasmonic nanostructures have been demonstrated in many schemes, such as metamaterials,[8–14] graphene structures,[15–20] metal nanowire grating-coupled dielectric waveguides,[21] and metal photonic crystals.[22] The metal–dielectric–metal (MDM) plasmonic waveguide side-coupling cavity has elicited widespread attention because it can achieve on-chip PIT effects.[23–26] In addition, plasmonic waveguide side-coupling cavity structures can be easily fabricated on integrated photonic chips. However, researchers have rarely studied slow light in MDM plasmonic waveguide platforms by using aperture-coupled disk resonators.

Conventional realization of PIT effect and slow light is achieved by adjusting the structural parameters of plasmonic nanostructures, such as the metal damping factor, resonator diameter, and coupling distance.[4] Once the geometric parameters of these nanostructures are confirmed, the majority of plasmonic-coupled systems cannot actively control the PIT

*Project supported by the National Natural Science Foundation of China (Grant Nos. 11647122 and 61705064) and the Natural Science Foundation of Hubei Province, China (Grant Nos. 2018CFB672 and 2018CFB773).

†Corresponding author. E-mail: wangboyun913@126.com
‡Corresponding author. E-mail: yuhuaqing@126.com

© 2020 Chinese Physical Society and IOP Publishing Ltd

effect. As a static system, this type of nanostructure is limited by the bandwidth–delay product. The operating bandwidth is conversely proportional to the maximal accomplishable group delay.[27] This limitation of the bandwidth–delay product can be overcome through the dynamic adjustment of the PIT effect and slow light in a coupled nanocavity system. However, achieving ultrafast and low-power dynamically adjustable PIT effects and slow light on the nanophotonic devices remain challenging.

Many integrated photonic devices need a dynamically adjustable PIT effect and slow light, that is, the peak wavelength, the size of the PIT window, and the group index change with the structure parameters. Yang *et al*. reported an on-chip adjustable PIT effect in four plasmonic comb cavities coupled waveguide system. The cavities were overlaid by a 100 nm thick poly(methy1 methacrylate) (PMMA) layer.[28] The response time of PMMA was in the microsecond range. Therefore, the third-order nonlinear Kerr effect was used to realize subpicosecond or even femtosecond ultrafast response time. In addition, Lu *et al*. and Pu *et al*. researched resonators and MDM waveguides full of nonlinear Kerr material AgBaO.[29,30] On the basis of the considerably small third-order nonlinear susceptibility of the traditional optical Kerr material, the threshold pump light intensity can be as high as 1 GW/cm^2. For dynamically adjustable slow light, the conventional implementation method involves adjusting the propagation phase of the plasmonic waveguide in a coupled waveguide system or using radiative and subradiant meta-atoms in a metamaterial structure. Han *et al*. have studied ultrafast, low-power, dynamically tunable slow light in an MDM waveguide coupled to cavity systems with nonlinear optical Kerr material.[24] The dynamic adjustment of the propagation phase of the plasmonic waveguide led to a pump light intensity of 11.7 MW/cm^2 and a group index of up to 14.5. In addition, Zhu *et al*. have reported an all-optical PIT effect in metamaterials coated on ITO layers.[31] Hence, only a few studies have implemented ultrafast, low-power, dynamically adjustable PIT effects and slow light in plasmonic waveguide coupling systems through the dynamic adjustment of the frequency of the nanocavity and the propagation phase of the plasmonic waveguide.

Graphene is a single-layer carbon atom arranged in a bidimensional honeycomb lattice. The excellent electrical and optical properties of graphene endow this material a potential for application in photonic devices. Graphene has a large effective third-order nonlinear susceptibility $\chi^{(3)}$ in the visible and near-infrared range, which has been validated through FWM[32] and Z-scan tests.[33] This distinct capability makes graphene a suitable material for the development of different tunable nanophotonic devices.[26] Therefore, the conventional nonlinear optical Kerr material is replaced with graphene to decrease the intensity of the pump light and to achieve low-power slow light in our study.

In this work, we investigate an ultrafast and low-power slow light tuning mechanism in PIT system through the dynamic adjustment of the frequency of the disk cavity and the propagation phase of the plasmonic waveguide. The simulation results indicate that when a single-layer graphene is used in the PIT system, the group velocity is controlled between $c/53.2$ and $c/2.8$ (c is the speed of light in vacuum). The numerical results show that the footprint of the PIT system is less than 0.8 μm^2. Graphene can achieve response time in the order of 1 ps to tune an ultrafast response slow light. Thus, the provided ultracompact PIT structure has potential applications for slow light and dynamic light storage devices.

The rest of this paper is arranged as follows. Section 2 shows the slow light tuning mechanism through the adjustment of the frequency mistuning of the disk cavities. Section 3 presents another slow light tuning mechanism through the adjustment of the propagation phase of the plasmonic waveguide. Section 4 summarizes the paper.

2. Frequency mistuning of nanocavities for tuning the slow light of the PIT effect

Figure 1 presents a diagram of two disk resonators with apertures linked to an MDM plasmonic waveguide system. The metal is Ag, and the insulator is air. Disk cavity 1 is overlaid by single-layer graphene (assumed to be 0.5 thick nm in this study). For simulation convenience, single-layer graphene is covered on the upper part of the photonic device, as shown in Fig. 1. In all simulations, the width and length of the coupling aperture are maintained at 20 nm and 55 nm, respectively. The width w of the plasmonic waveguide is 50 nm. The coupling distance L between the two disk cavities is 281 nm. d_1 and d_2 are the diameters of disk cavities 1 (393 nm) and 2 (395 nm), respectively. The resonant wavelength of the disk cavities can be determined by tuning their diameters. Notably, small diameter mistuning ($\Delta d = |d_1 - d_2|$) can cause a narrow bandwidth and a low transparent window amplitude.[24] This conclusion is conducive to adjusting the PIT effect and slow light. However, active control of slow light cannot be achieved because the geometric parameters of the structure are confirmed. In this study, single-layer graphene is covered on the upper part of the photonic device; thus, the resonant wavelength of disk cavity 1 can be dynamically adjusted by pump light with different intensities.

Figure 1 indicates that the two disk cavities are assembled on two sides of the plasmonic waveguide, and a single-layer graphene covers disk cavity 1. When transverse magnetic polarized light is incident and coupled to a plasmonic waveguide, SPPs waves are formed on the metal surface and are limited at the metal–dielectric interface. Samples of a U-shaped plasmonic waveguide (Fig. 1) are linked by two disk cavities on

two sides. The U-shaped plasmonic waveguides can be fabricated using an experimental method on silica substrates.[26] The thickness of the Ag membrane is 300 nm, and the depth of the U-shaped plasmonic waveguide and two disk cavities is set to 150 nm.

The Kerr nonlinear material is chosen as graphene in our work. Graphene films were grown on copper substrates by chemical vapor deposition (CVD) using methane in Ref. [34]. The dry transfer technique can be used to transfer graphene films onto the entire PIT system. First, relatively thick PMMA was coated on a graphene/copper foil. A polydimethylsiloxane (PDMS) block with a through hole in the center was attached to the PMMA/graphene/copper films by natural adhesion. The copper was then etched while the PDMS/PMMA/graphene block was floating over the solution. Using the PDMS "handle", the composite was easily rinsed and dried after etching, thereby removing the liquid used in the etching process. Next, the PDMS/PMMA/graphene composite was placed onto the target substrate, covering the entire PIT system. The substrate was heated. The heat treatment allowed the wavy and rough PMMA/graphene film to make full contact with the target substrate. After heating, the adhesion of the graphene to the substrate was strong enough to peel off the PDMS block without delaminating the PMMA/graphene film. Finally, the PMMA was thermally removed in a furnace, without the use of any solvent. The graphene film was transferred onto the entire PIT system. At this time, the graphene film was covered on the entire PIT system. The graphene film that was covered on other areas except the areas of the upper part of the photonic device and the MDM plasmonic waveguide between the two disk resonators was etched by adopting inductively coupled plasma (ICP) etching process.[35] Hence, the graphene film was covered on the upper part of the photonic device (Fig. 1) and the MDM plasmonic waveguide between the two disk resonators (Fig. 6).

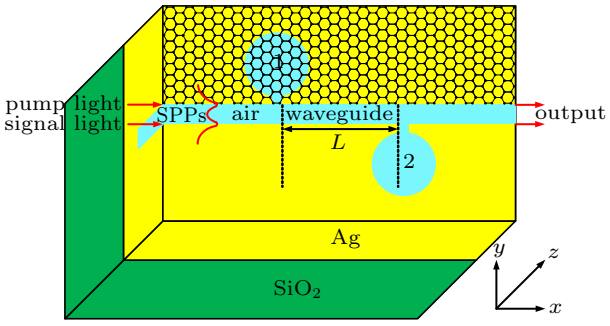


Fig. 1. Diagram of two disk cavities with apertures linked to a plasmonic waveguide system with frequency mistuning between the two disk cavities. Disk cavity 1 is overlaid by the optical Kerr nonlinear material single-layer graphene.

The dynamic transmitted features of the plasmonic structure can be analyzed on the basis of coupled mode theory in accordance with frequency mistuning and phase shift between the two disk cavities. The dynamic formula of the cavity pattern amplitude y_i of the i-th cavity ($i = 1, 2$) can be expressed as[36]

$$\frac{\mathrm{d}y_1}{\mathrm{d}t} = (-\mathrm{j}\omega_1 - \kappa_{\mathrm{int},1} - \kappa_{\mathrm{c},1})y_1 + \mathrm{e}^{\mathrm{j}\theta_1}\sqrt{\kappa_{\mathrm{c},1}}x^{(1)}_{+,\mathrm{in}} + \mathrm{e}^{\mathrm{j}\theta_1}\sqrt{\kappa_{\mathrm{c},1}}x^{(1)}_{-,\mathrm{in}}, \tag{1}$$

$$\frac{\mathrm{d}y_2}{\mathrm{d}t} = (-\mathrm{j}\omega_2 - \kappa_{\mathrm{int},2} - \kappa_{\mathrm{c},2})y_2 + \mathrm{e}^{\mathrm{j}\theta_2}\sqrt{\kappa_{\mathrm{c},2}}x^{(2)}_{+,\mathrm{in}} + \mathrm{e}^{\mathrm{j}\theta_2}\sqrt{\kappa_{\mathrm{c},2}}x^{(2)}_{-,\mathrm{in}}, \tag{2}$$

where $x^{(i)}_{p,\mathrm{in}}$ and $x^{(i)}_{p,\mathrm{out}}$ ($i = 1, 2$) represent the incident and output waves in the bus waveguide, respectively. The subscript $p = \pm$ indicates two directions of propagation, as indicated in Fig. 2. ω_i ($i = 1, 2$) is the resonance frequency of the i-th disk cavity, $\kappa_{\mathrm{int},i} = 1/\tau_{\mathrm{int},i} = \omega_i/(2Q_{\mathrm{int},i})$ is the attenuation ratio caused by the intrinsic attenuation in the i-th disk cavity, and $\kappa_{\mathrm{c},i} = 1/\tau_{\mathrm{c},i} = \omega_i/(2Q_{\mathrm{c},i})$ is the attenuation ratio caused by the escape of energy into the bus waveguide. $Q_{\mathrm{int},i}$ and $Q_{\mathrm{c},i}$ are quality factors related to intrinsic attenuation and waveguide coupling loss, respectively. θ_i is the phase of the coupling factor.

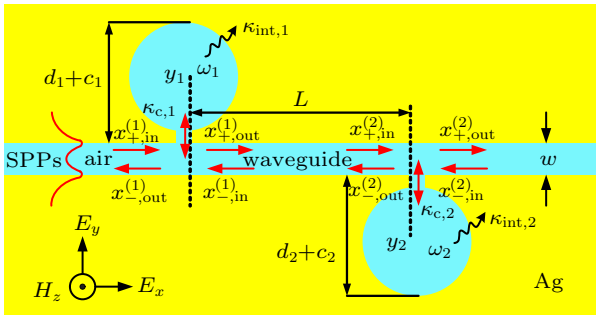


Fig. 2. Diagram of a simple system model to achieve the PIT effect.

For simplicity, we suppose that only one incoming light ($x^{(2)}_{-,\mathrm{in}} = 0$) exists in the PIT system. The transmitted and reflection coefficients of the PIT system can be concluded as

$$t_i(\omega) = \frac{\mathrm{j}(\omega_i - \omega) + \kappa_{\mathrm{int},i}}{\mathrm{j}(\omega_i - \omega) + \kappa_{\mathrm{int},i} + \kappa_{\mathrm{c},i}}, \tag{3}$$

$$r_i(\omega) = -\frac{\kappa_{\mathrm{c},i}}{\mathrm{j}(\omega_i - \omega) + \kappa_{\mathrm{int},i} + \kappa_{\mathrm{c},i}}. \tag{4}$$

The phase of the coupled factor is as assumed to be 0, which refers to $\theta_1 = \theta_2 = 0$. For the PIT system, the output transmitted efficiency can be calculated as

$$T = |t|^2 = \left|\frac{x^{(2)}_{+,\mathrm{out}}}{x^{(1)}_{+,\mathrm{in}}}\right|^2 = \left|\frac{t_1(\omega)t_2(\omega)}{1 - r_1(\omega)r_2(\omega)\,\mathrm{e}^{\mathrm{j}\phi}}\right|^2, \tag{5}$$

where ϕ is the round-trip phase shift between the two disk cavities. The round-trip phase shift of the system can be expressed as $\phi = 2m\pi + 2\Delta\phi$ (where m is an integer and $\Delta\phi$ is the unidirectional phase shift of the system). Here, only $\Delta\phi$ is considered when calculating the round-trip phase shift of the

system. The effective phase shift of the transmitted spectrum $\varphi(\omega)$ and group delay τ_g can be calculated as $\varphi(\omega) = \arg(t)$ and $\tau_g = \partial\varphi(\omega)/\partial\omega$, respectively.[37] The slow light effect can be expressed by group index n_g, which is given as

$$n_g = \frac{c}{v_g} = \frac{c}{l}\tau_g = \frac{c}{l}\cdot\frac{\partial\varphi(\omega)}{\partial\omega}, \tag{6}$$

where v_g represents the group velocity, c is the speed of light in vacuum, and $l = 1$ μm is the length of the plasmonic system.

Electrical or optic modulation methods related to the heating effect have been used in many studies.[38,39] The modulation velocity of the heating effect is too low. In addition, the heating effects of nonlinear adsorption can interfere with the nonlinear dynamics if they are not correctly controlled. Numerous dynamic tuning mechanisms are available for photonic nonlinear devices, and these include slow light tuning with ultrafast response time and low pump power. An ultrafast response time can be achieved through optical Kerr modulation, and low pump power can be obtained by applying different nonlinear Kerr materials. Han *et al.* reported ultrafast, low-power, all-optical tunable PIT in an MDM waveguide side-coupled Fabry–Perot resonator system with a nonlinear organic polymer.[40] The intensity of the pump beam is high (i.e., usually about several gigawatts per square centimeter) because the third-order nonlinear susceptibility of organic polymers is small. The large pump power of the optical Kerr material restricts the use of integrated photonic devices.

Compared with the conventional Kerr nonlinear material, graphene has larger effective third-order Kerr coefficient. Gu *et al.* showed in experiments that graphene has a very high third-order nonlinear response.[41] Zhu *et al.* indicated that the linear refractive exponent of graphene is $n_0 = 2.4$, and the large Kerr nonlinear coefficient is $n_2 = -1.2\times10^{-7}$ cm^2/W, which is four orders of magnitude greater than that of nonlinear organic polymers.[26] The variation in the Kerr-induced refractive exponent is defined as $\Delta n = n_{2\text{eff}}I$, where $n_{2\text{eff}}$ is the effective Kerr nonlinear coefficient and I is the pump light intensity. In this study, the graphene–Ag compound material structure has a large effective Kerr nonlinear coefficient of $n_{2\text{eff}} \approx n_2$. The effective refractive exponent n of graphene is indicated as $n = n_0 + n_{2\text{eff}}I \approx n_0 + n_2 I$.

In addition, Nikolaenko *et al.* demonstrated that an ultrafast response time of about 1 ps can be achieved in graphene.[42] Reckinger *et al.* also indicated that the resonant performance of plasmonic waveguide is affected by the refractive exponent of surrounding dielectric materials.[43] When a single-layer graphene is covered on the surface of a cavity or waveguide, the refractive exponent of the surrounding dielectric material varies. Such variation influences the resonant wavelength of the nanocavity and the phase shift of the plasmonic waveguide.

The total quality factor Q_t of the disk cavity can be calculated from $Q_t = \lambda_0/\Delta\lambda$, where λ_0 and $\Delta\lambda$ are the peak wavelength and full width at half maximum of the reflection spectrum, respectively. If $Q_{\text{int}} \gg Q_c$, the coupling quality factor can be calculated from the formula $Q_c = Q_{\text{int}}Q_t/(Q_{\text{int}} - Q_t)$. When the diameters of disk cavities 1 and 2 are set to 393 nm and 395 nm, respectively, Q_{int} is about 530. The finite-difference time-domain (FDTD) simulation shows that Q_t is approximately 65. Therefore, Q_c is approximately 74.1. For the FDTD simulation, the time precision is set to 3000 fs and perfectly matched layer conditions are used to simulate. The steps of space and time are set to $\Delta x = \Delta y = 2$ nm and $\Delta t = \Delta x/2c$, respectively.

The frequency mistuning of the nanocavity is controlled by adjusting the resonant wavelength of the disk cavity. A pump beam with a wavelength of 830 nm is used. The FDTD simulation indicates that the resonant wavelength of disk cavity 2 is 788 nm. Disk cavity 1 is overlaid by a single-layer graphene. The effective refractive exponent of the graphene–Ag compound material structure is varied by using optical Kerr modulation. The resonant wavelength of disk cavity 1 is determined to $\lambda = 40.65(n_0 + \Delta n) + 690.44$ nm via direct numerical modeling of the cavity.

The change in the resonance wavelength of the disk cavity under various pump light intensities when disk cavity 1 is overlaid by a single-layer graphene is shown in Fig. 3. The variation in the resonant wavelength increases with the increase in pump light intensity and presents a linear tendency. The effective Kerr nonlinear coefficient n_2 is a negative value; consequently, the effective refractive exponent of graphene decreases under the excitation of the pump beam, which causes a blue shift in the resonant wavelength of the disk cavity. Hence, the resonant wavelength of disk cavity 1 shifts to the short wavelength direction. When the pump light intensity increases from 0 MW/cm^2 to 2.46 MW/cm^2, the variation in the resonant wavelength is 12 nm. This result means that the slow light can be dynamically adjusted over a wide wavelength range of 12 nm through a frequency mistuning mechanism. These findings indicate the probability of achieving tunable, low-power, ultrafast, slow-light in integrated optical circuits.

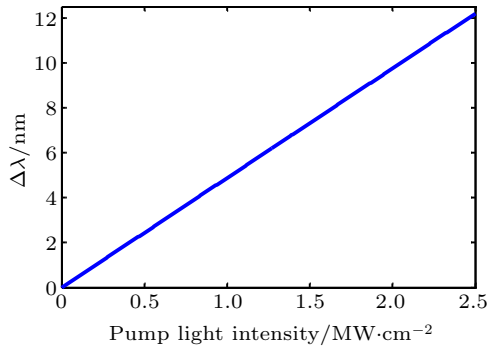


Fig. 3. Relationship between the variation in the resonant wavelength of a disk cavity and the pump light intensity.

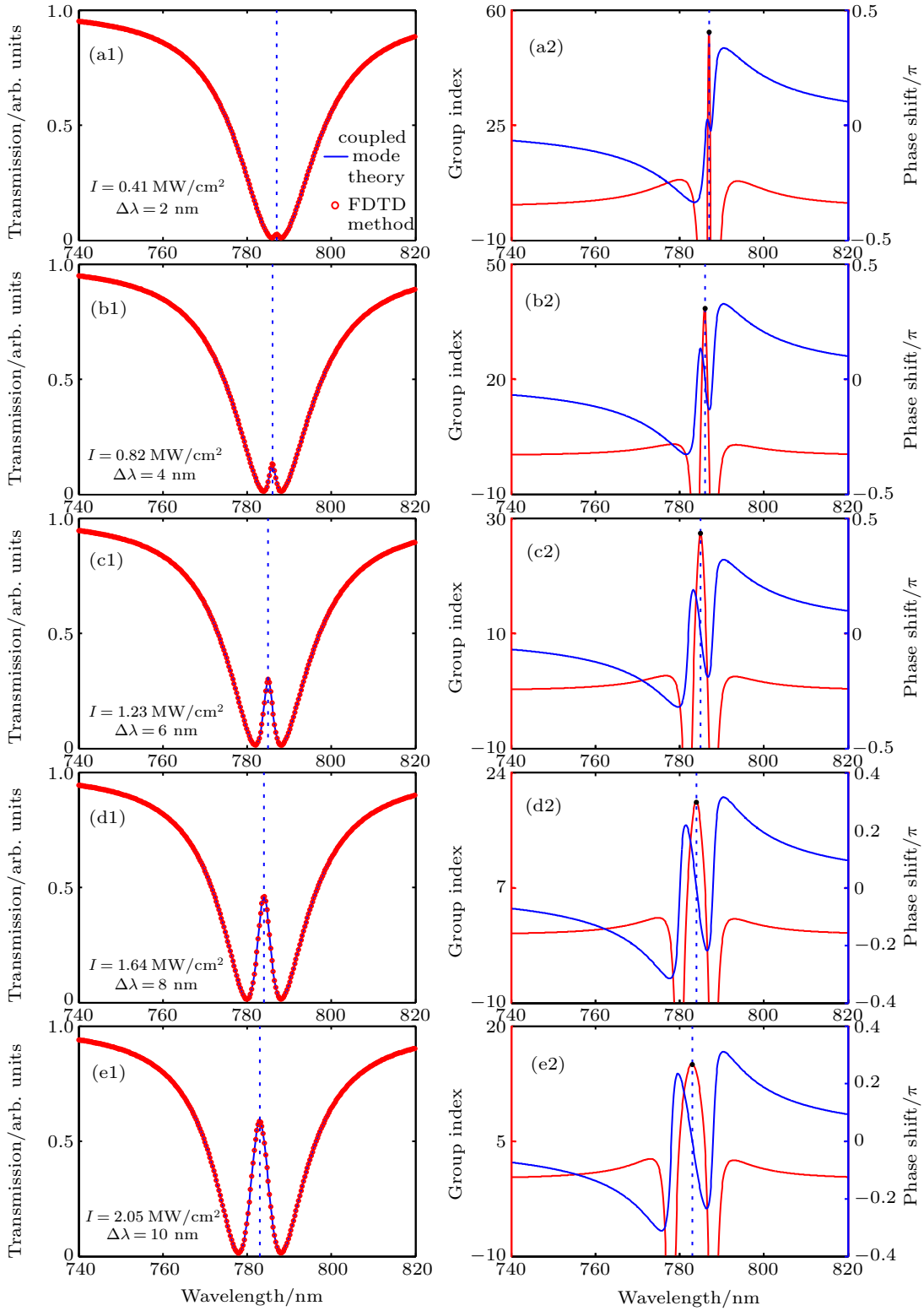


Fig. 4. Transmitted spectra (a1)–(e1), transmitted phase shift responses and group indices (a2)–(e2) under various pump light intensities when disk cavity 1 is overlaid by a graphene layer with a thickness of 0.5 nm. The black dots stand for the group indices of the PIT peaks with values of 53.2, 38.8, 27.5, 19.8, and 15.1.

Figure 4 shows the transmitted spectrum, the transmitted phase shift response, and the group indices under different intensities of the pump beam (from 0.41 MW/cm^2 to 2.05 MW/cm^2). The distance L between the two disk cavities is set to 281 nm. The red circle denotes the FDTD simulation result, and the solid blue line denotes the theoretical result obtained using formula (5). In our simulations, the effective refractive exponent n_{eff} of graphene is related to the pump light intensity I. When the effective refractive exponent of graphene is fixed, the effective refractive exponent n_{eff} of the excited SPPs wave changes with the alteration of the incident frequency.[44–47] The transmission intensity spectral re-

sponses in our PIT system for different refractive exponents of graphene are researched. As the intensity of the pump beam increases, the resonant wavelength of disk cavity 1 is blue-shifted, and the resonant mistuning between the two cavities widens. The PIT transparent wavelength blue-shifts due to the negative value of the effective Kerr nonlinear coefficient n_2. The transmitted spectrum shows a symmetrical PIT peak because the strong coupling is met or the round-trip phase shift ϕ is $2m\pi$ (where m is an integer). Figures 4(a2)–4(e2) show that the transmitted phase shift at the transparent wavelength is 0π because the Fabry–Perot resonant condition is met.

Figures 4(a1)–4(e1) show that as wavelength mistuning $\Delta\lambda$ increases, the transparent peak gradually widens, indicating that the coherent interference between the two disk cavities increases. Figure 4(a1) demonstrates that when the pump light intensity is 0.41 MW/cm^2, the wavelength mistuning is 2 nm, and a low PIT peak is observed. When the pump light intensity is increased to 2.05 MW/cm^2, the wavelength mistuning is 10 nm, and the peak value of PIT reaches 60%, as shown in Fig. 4(e1). This means that strong coherent interference is obtained between the two disk cavities.

This PIT system is considerably restrained by the delay–bandwidth product; the maximal accomplishable delay is conversely proportional to the operation bandwidth. That is, a tradeoff exists between frequency mistuning and group index. Hence, as indicated in Figs. 4(a2)–4(e2), the group index at the transparent wavelength decreases as the frequency mistuning increases. Meanwhile, as the group index increases, the intensity of the PIT transparent peak decreases. The reason is that as the signal light spends more time in both disk cavities, more light power is lost by scattering in the cavities. The maximal group index is 53.2. This value is 15 times larger than the sum of the group indexes of the waveguide and cavity. This excessive group index shows that the two disk cavities do interfere. The group indexes of the transparent wavelength are 53.2, 38.8, 27.5, 19.8, and 15.1 at the pump light intensities of 0.41 MW/cm^2, 0.82 MW/cm^2, 1.23 MW/cm^2, 1.64 MW/cm^2, and 2.05 MW/cm^2, respectively.

Figure 5 indicates the relationship between the group velocity and pump light intensity to visualize the physical mechanism of the dynamic tunable slow light. According to the above analysis, $v_g = c/n_g$; the group velocity is inversely proportional to the group index. The group velocity increases with increasing pump light intensity. The group velocity is controlled between $c/53.2$ and $c/15.1$ through the dynamic adjustment of the resonance wavelength when disk cavity 1 is covered by a graphene layer with a thickness of 0.5 nm. The minimum group velocity is $c/53.2$ and a good slow light can be obtained, but the intensity of the PIT peak is only approximately 2.7% in Fig. 4(a1). This particular result indicates that the transmission intensity is too weak and that more light energy is lost due to scattering in the disk cavities. The pump light intensity is higher than 0.82 MW/cm^2, the intensity of the PIT peak exceeds 13.3% in Fig. 4, and the group velocity can be as low as $c/38.8$ in Fig. 5. Therefore, when the pump light intensity is controlled between 0.82 MW/cm^2 and 2.05 MW/cm^2, a trade-off exists between the group velocity and the transmission intensity. The pump light intensity should be controlled between 0.82 MW/cm^2 and 2.05 MW/cm^2 to decrease the power and achieve a slow group velocity, which indicates significant application potential in tunable, low-power, and ultrafast slow light devices.

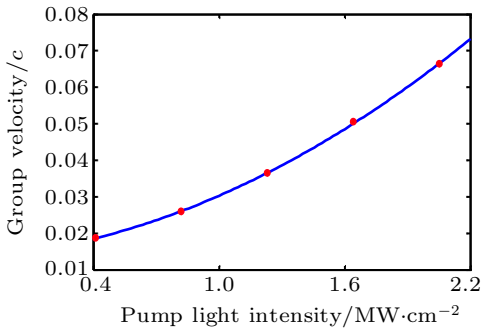


Fig. 5. Relationship between the group velocity and the pump light intensity under frequency mistuning for tuning slow light.

3. Propagating phase of the plasmonic waveguide for tuning the slow light of the PIT effect

Figure 6 presents a diagram of two disk cavities with apertures linked to an MDM plasmonic waveguide system. A single-layer graphene covers a plasmonic waveguide between the two disk cavities. The diameters of disk cavities 1 and 2 are set to 394 nm and 400 nm, respectively. The distance L between the two disk cavities is 281 nm. The background metal is Ag. Its frequency-related complex relative dielectric constant can be determined using the well-known equation $\varepsilon_m(\omega) = \varepsilon_\infty - \omega_p^2/(\omega^2 + j\omega\gamma_p)$ and $(\varepsilon_\infty, \omega_p, \gamma_p) = (3.7, 9.1\text{ eV}, 0.018\text{ eV})$, where ε_∞ is the permittivity at infinite frequency, ω_p is the bulk frequency, and γ_p is the damping ratio.[36]

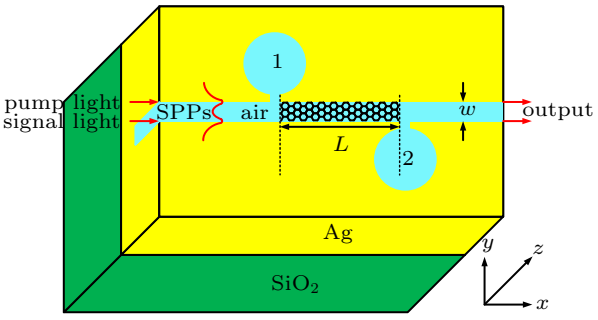


Fig. 6. Diagram of two disk cavities with apertures linked to a plasmonic waveguide system and with the propagating phase detuned between the two disk cavities. The plasmonic waveguide between the two cavities is overlaid by the optical Kerr nonlinear material single-layer graphene.

With the dispersion of the plasmonic waveguide, the cavity–cavity phase shift $\Delta\phi_1$ can be expressed as $\Delta\phi_1 =$

$\omega_s \mathrm{Re}(n_{\mathrm{eff}})L/c$, where ω_s is the frequency of the signal light. n_{eff} is the effective refractive exponent and can be acquired by using the dispersion formula[36]

$$\tanh\left(\frac{w\pi\sqrt{n_{\mathrm{eff}}^2-\varepsilon_d}}{\lambda}\right)=-\frac{\varepsilon_d\sqrt{n_{\mathrm{eff}}^2-\varepsilon_m}}{\varepsilon_m\sqrt{n_{\mathrm{eff}}^2-\varepsilon_d}}, \tag{7}$$

where ε_m and ε_d represent the dielectric constants of the metal and the dielectric waveguide with a width of $w = 50$ nm, respectively. The dielectric is set to air, and the dielectric constant of air is 1 ($\varepsilon_d = 1$).

Figure 7 shows a phase shift that meets the dispersion formula as a function of wavelength. When the wavelength is increased to 789 nm, a π phase shift is acquired in the MDM plasmonic waveguide. When $\lambda = 2[\mathrm{Re}(n_{\mathrm{eff}})]L = 2\times 1.404\times 281 \approx 789$ nm, $\Delta\phi_1$ is equal to π. Figure 7 also shows that when the distance between the two disk cavities is 281 nm, the optimal wavelength is 789 nm, which is in good agreement with the parameter settings.

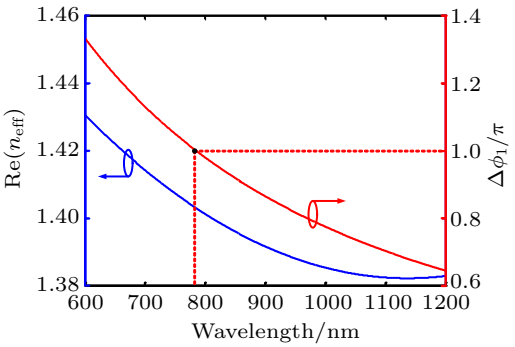


Fig. 7. Real part of the effective refractive exponent and phase shift satisfying the dispersion formula in a plasmonic waveguide with $w = 50$ nm. The black dot indicates the value of π that meets the dispersion formula at $\lambda = 789$ nm.

Details on the other structural parameters of the PIT systems are provided in this work. FDTD simulation shows that the resonant wavelengths of cavities 1 and 2 are 784 nm and 794 nm, respectively. The transparent wavelength is 789 nm.

The group index of PIT can be controlled by adjusting the propagation phase of the plasmonic waveguide with an 830 nm pump beam. In the dynamic situation, with optical Kerr effect, the effective refractive exponent variation causes the effective phase shift of the waveguide signal light $\Delta\phi_2 = 2\pi\Delta n_{\mathrm{eff}}L/\lambda_s$, where Δn_{eff} is the variation of the effective refractive exponent caused by the Kerr effect, $\Delta n_{\mathrm{eff}} \approx \Delta n$, and λ_s is the wavelength of the signal light. In this work, when the pump light intensities are 5.88 MW/cm^2 and 11.76 MW/cm^2, the phase shifts of the signal light are 0.5π and π, respectively.

Thus, a portion of the phase shift between the two disk cavities stems from the dispersion of the SPPs wave in a static situation; the other portion is based on optical Kerr effect in the plasmonic waveguide in a dynamic situation. The unidirectional phase shift of the system (e.g., cavity–cavity phase shift) can be indicated as $\Delta\phi = \Delta\phi_1 + \Delta\phi_2$. The effective Kerr nonlinear coefficient of graphene is negative, and the phase shift of the signal light is reduced, which means $\Delta\phi_2 < 0$. Cavity–cavity phase shift $\Delta\phi$ can be tuned from π to 0 as the pump light intensity increases from 0 MW/cm^2 to 11.76 MW/cm^2 when $\Delta\phi_1$ equals π.

Figure 8 presents the calculated transmitted spectrum, transmitted phase shift response, and group index under different pump beam intensities (from 0 MW/cm^2 to 11.76 MW/cm^2). The red circle is the FDTD simulation result, and the solid blue line is the theoretical result obtained using formula (5). The theoretical results agree with the FDTD simulation results. When the phase shift between the two disk cavities is adjusted to π, the maximum PIT transmitted peak is created. The phase shift of the transmitted spectrum is varied by 2π (Figs. 8(a2)–8(e2)) because the optical Kerr effect reduces the effective refractive exponent of the plasmonic waveguide. Thus, phase shift multiplication of the PIT effect is observed. In addition, the system's round-trip phase is $2m\pi$, which leads to Fabry–Perot resonance. Figures 8(a2) and 8(e2) show that the maximal group index of the PIT window can reach 14.8, which indicates that much time is spent between the two cavities.

Figures 8(a1) and 8(b1) show that when $\Delta\phi \in [\pi, 0.5\pi)$, the PIT transmitted window is blue-shifted, and the transmitted intensity is decreased. Figures 8(c1) and 8(d1) demonstrate that when $\Delta\phi \in [0.5\pi, 0)$, the PIT transmitted window is red-shifted, and the transmitted intensity is increased. The system's round-trip phase is adjusted away from $2m\pi$, leading to asymmetrical Fano-like transmitted spectra (Figs. 8(b1) and 8(d1)) and group index spectra (Figs. 8(b2) and 8(d2)), which are caused by unsatisfactory coupling interference between the two disk cavities. The group index at the transparent wavelength is 7.9. When $\Delta\phi = 0.5\pi$, the coupling between the two disk cavities is the weakest and has the minimum value in the transmitted spectrum (Fig. 8(c1)) due to the Fabry–Perot resonance. Figures 8(c1) and 8(c2) indicate that the minimum transmitted intensity and the group index of the transparent wavelength at 789 nm ($n_g = 2.8$) are obtained. The phase shifts of the transparent wavelength at 789 nm are -2π, -1.48π, $-\pi$, -0.27π, and 0π (Figs. 8(a2)–8(e2)). When the pump light intensities are 0 MW/cm^2, 1.77 MW/cm^2, 5.88 MW/cm^2, 9.99 MW/cm^2, and 11.76 MW/cm^2, the group indexes of the transparent wavelength at 789 nm are 14.8, 7.9, 2.8, 7.9, and 14.8, respectively (Figs. 8(a2)–8(e2)).

The distributions of $|H_z|^2$ are calculated at two dip wavelengths and at the transmitted peak wavelength via FDTD simulation to illustrate the physical cause of the PIT phenomenon. The results are presented in Figs. 9(a)–9(c). Both disk cavities function as a resonator, and Fabry–Perot resonance exists between the two cavities.

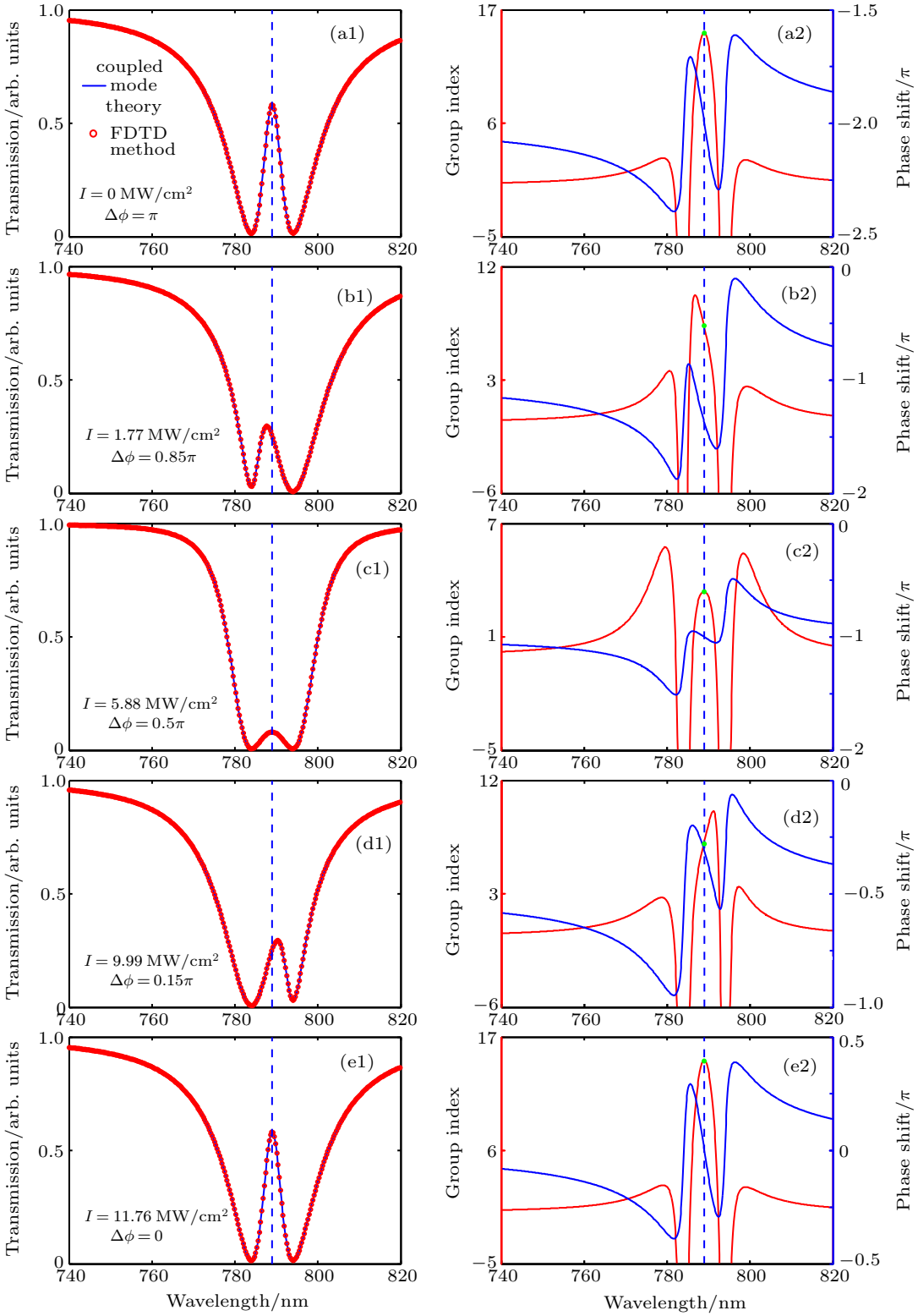


Fig. 8. Transmitted spectra (a1)-(e1), transmitted phase shift responses and group indices (a2)-(e2) at diverse pump light intensities when the plasmonic waveguide between the two disk cavities is covered by a 0.5 nm thick graphene layer. The green dots stand for the group index of the transparent wavelength at 789 nm with values of 14.8, 7.9, 2.8, 7.9, and 14.8.

Figure 10 shows the relationship between the group velocity and pump light intensity. The group velocity increases with the increase in pump light intensity but decreases when the system round-trip phase is π (i.e., the pump light intensity is 5.88 MW/cm^2). The group velocity of the PIT system is affected by the coupling strength between the two cavities. When the pump light intensity is 5.88 MW/cm^2 (i.e., $\Delta\phi = 0.5\pi$), the weak coupling interference condition between the two cavities is met. The maximal group velocity can reach $c/2.8$. Therefore, almost no coherent interference occurs between the two disk cavities, and the delay is basically induced by a direct path delay. When the pump light

intensity is increased to 11.76 MW/cm^2, the strong coupling interference condition between the two cavities is satisfied. The minimum group velocity is $c/14.8$. The strong dispersion around the transparency window leads to a slow group velocity. The coherent effect between the two cavities is the strongest, which indicates that more time is spent in the disk cavities. Therefore, the group velocity is controlled between $c/14.8$ and $c/2.8$ through the dynamic adjustment of the propagation phase of the plasmonic waveguide. This finding implies that a large tuning range of the group velocity can be achieved in the proposed PIT system. These results reveal the possibility of application in dynamically tunable, low-power, slow light devices.

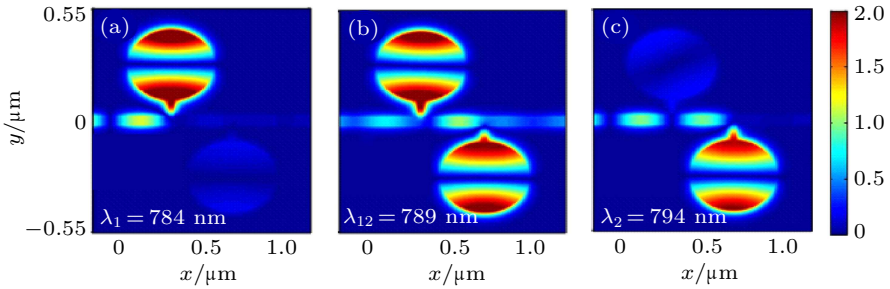


Fig. 9. Distribution of $|H_z|^2$ at dip wavelengths of 784 nm (a) and 794 nm (c) and transparent wavelength of 789 nm (b) under a pump light intensity of 11.76 MW/cm^2. The relevant transmitted spectrum is shown in Fig. 8(e1).

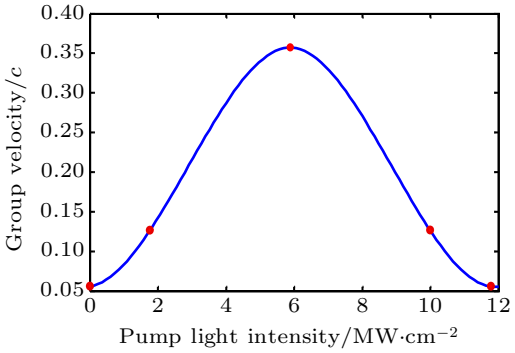


Fig. 10. Relationship between the group velocity and the pump light intensity under the propagation phase of the plasmonic waveguide slow-light tuning mechanism.

4. Conclusions

An ultrafast and low-power slow light tuning mechanism based on the PIT effect in two disk cavities aperture-coupled to an MDM plasmonic waveguide system with a nonlinear optical Kerr material is investigated via theoretical and simulation methods. The group velocity is maintained between $c/53.2$ and $c/15.1$ with increasing pump light intensity from 0.41 MW/cm^2 to 2.05 MW/cm^2 by dynamic adjustment of the resonant frequency of the disk nanocavity via fine tuning of the group velocity. Meanwhile, the group velocity is maintained between $c/2.8$ and $c/14.8$ with increasing pump light intensity from 5.88 MW/cm^2 to 11.76 MW/cm^2; these can achieve a large tuning range of the group velocity by dynamic adjustment of the propagation phase of the plasmonic waveguide. The graphene–Ag compound material structure decreases the pump intensity because the local EM field of SPPs and slow light enhances the optical Kerr effect. Moreover, phase shift multiplication of the PIT effect is observed. The simulation results indicate that the entire structure is very compact, occupying less than 0.8 μm^2, and can achieve ultrafast response time in the order of 1 ps. The outcomes may pave the way for the design and fabrication of nanoscale supersensitive sensors, tunable slow-light devices, low-power optical storage, and ultrafast nonlinear devices in highly photonic integrated circuits.

References

[1] Boyd R W and Gauthier D J 2006 *Nature* **441** 701
[2] Kekatpure R D, Barnard E S, Cai W and Brongersma M L 2010 *Phys. Rev. Lett.* **104** 243902
[3] Qin M, Wang L L, Zhai X, Lin Q and Xia S X 2018 *IEEE Photon. Techno. Lett.* **30** 1009
[4] Han X, Wang T, Li X M, Liu B, He Y and Tang J 2015 *IEEE J. Lightwave Techno.* **33** 3083
[5] Zhang S, Genov D A, Wang Y, Liu M and Zhang X 2008 *Phys. Rev. Lett.* **101** 047401
[6] Wang T, Zhang Y S, Hong Z and Han Z H 2014 *Opt. Express* **22** 21529
[7] Jia W, Ren P W, Tian Y C and Fan C Z 2019 *Chin. Phys. B* **28** 026102
[8] Yan X, Wang T, Xiao S, Liu T, Hou H, Cheng L and Jiang X 2017 *Sci. Rep.* **7** 1
[9] Tian Y C, Jia W, Ren P W and Fan C Z 2018 *Chin. Phys. B* **27** 124205
[10] Ling Y, Huang L, Hong W, Liu T, Luan J, Liu W, Lai J and Li H 2018 *Nanoscale* **10** 19517
[11] Xiao S, Wang T, Liu T, Yan X, Li Z and Xu C 2018 *Carbon* **126** 271
[12] Zhang B, Li H, Xu H, Zhao M, Xiong C, Liu C and Wu K 2019 *Opt. Express* **27** 3598
[13] Liu C, Li H, Xu H, Zhao M, Xiong C, Zhang B and Wu K 2019 *J. Phys. D: Appl. Phys.* **52** 405203
[14] Zhao W, Qi J, Lu Y, Wang R, Zhang Q, Xiong H, Zhang Y, Wu Q and Xu J 2019 *Opt. Express* **27** 7373
[15] Xiao S, Wang T, Jiang X, Yan X, Cheng L, Wang B and Xu C 2017 *J. Phys. D: Appl. Phys.* **50** 195101
[16] Xiao S, Wang T, Liu Y, Han X and Yan X 2017 *Plasmonics* **12** 185
[17] Yan S, Zhu X, Frandsen L H, Xiao S, Mortensen N A, Dong J and Ding Y 2017 *Nat. Commun.* **8** 14411
[18] Tang P, Li J, Du L, Liu Q, Peng Q, Zhao J, Zhu B, Li Z and Zhu L 2018 *Opt. Express* **26** 30655
[19] Xiang Y L, Zhai X, Lin Q, Xia S X, Qin M and Wang L L 2018 *IEEE Photon. Techno. Lett.* **30** 622
[20] Li H and Xu Y 2019 *Opt. Mater. Express* **9** 2107
[21] Xiao X, Tan Y, Guo Q, Li J, Liang S, Xiao S, Zhong H, He M, Liu L, Luo J and Chen L 2020 *Opt. Express* **28** 3136
[22] Li J, Chen Z, Yang H, Yi Z, Chen X, Yao W, Duan T, Wu P, Li G and Yi Y 2020 *Nanomaterials* **10** 257
[23] Han X, Wang T, Li X, Xiao S and Zhu Y 2015 *Opt. Express* **23** 31945
[24] Han X, Wang T, Li X, Liu B, He Y and Tang J 2015 *J. Phys. D: Appl. Phys.* **48** 235102

[25] Wang B, Zeng Q, Xiao S, Xu C, Xiong L, Lv H, Du J and Yu H 2017 *J. Phys. D: Appl. Phys.* **50** 455107
[26] Zhu Y, Hu X Y, Yang H and Gong Q H 2014 *Sci. Rep.* **4** 3752
[27] Li H, Chen B, Qin M and Wang L 2020 *Opt. Express* **28** 205
[28] Yang X Y, Hu X Y, Chai Z, Lu C C, Yang H and Gong Q H 2014 *Appl. Phys. Lett.* **104** 221114
[29] Lu H, Liu X, Wang L, Gong Y and Mao D 2011 *Opt. Express* **19** 2910
[30] Pu M, Yao N, Hu C, Xin X, Zhao Z, Wang C and Luo X 2010 *Opt. Express* **18** 21030
[31] Zhu Y, Hu X Y, Yang H and Gong Q H 2014 *Appl. Phys. Lett.* **104** 211108
[32] Hendry E, Hale P J, Moger J, Savchenko A K and Mikhailov S A 2010 *Phys. Rev. Lett.* **105** 097401
[33] Zhang H, Virally S, Bao Q L, Ping L K, Massar S, Godbout N and Kockaert P 2012 *Opt. Lett.* **37** 1856
[34] Li X, Cai W, An J, Kim S, Nah J, Yang D, Piner R, Velamakanni A, Jung I, Tutuc E, Banerjee S K, Colombo L and Ruoff R S 2009 *Science* **324** 1312
[35] Suk J W, Kitt A, Magnuson CW, Hao Y, Ahmed S, An J, Swan A K, Goldberg B B and Ruoff R S 2011 *ACS Nano* **5** 6916
[36] Lu H, Liu X and Mao D 2012 *Phys. Rev. A* **85** 053803
[37] Wei W Y, Yu Y F and Zhang Z M 2018 *Chin. Phys. B* **27** 034204
[38] Yang X, Yu M, Kwong D L and Wong C W 2010 *IEEE J. Sel. Top. Quantum Electron.* **16** 288
[39] Yang X, Yu M, Kwong D L and Wong C W 2009 *Phys. Rev. Lett.* **102** 173902
[40] Han X, Wang T, Wang B, Liu B, He Y and Zhu Y 2015 *J. Appl. Phys.* **117** 103105
[41] Gu T, Petrone N, McMillan J F, Zande A, Yu M, Lo G Q, Kwong D L, Hone J and Wong C W 2012 *Nat. Photon.* **6** 554
[42] Nikolaenko A E, Papasimakis N, Atmatzakis E, Luo Z, Shen Z X, Angelis F D, Boden S A, Fabrizio E D and Zheludev N I 2012 *Appl. Phys. Lett.* **100** 181109
[43] Reckinger N, Vlad A, Melinte S, Colomer J F and Sarrazin M 2013 *Appl. Phys. Lett.* **102** 211108
[44] Cen C, Chen Z, Xu D, Jiang L, Chen X, Yi Z, Wu P, Li G and Yi Y 2020 *Nanomaterials* **10** 95
[45] Cen C, Zhang Y, Chen X, Yang H, Yi Z, Yao W, Tang Y, Yi Y, Wang J and Wu P 2020 *Physica E* **117** 113840
[46] Li J, Chen X, Yi Z, Yang H, Tang Y, Yi Y, Yao W, Wang J and Yi Y 2020 *Materials Today Energy* **16** 100390
[47] Qin F, Chen X, Yi Z, Yao W, Yang H, Tang Y, Yi Y, Li H and Yi Y 2020 *Solar Energy Materials and Solar Cells* **211** 110535